Published in final edited form as:
Nat Neurosci. 2013 February ; 16(2): 210–218. doi:10.1038/nn.3305.

The organization of two novel cortical interneuronal circuits

Xiaolong Jiang[1,4], **Guangfu Wang**[1,4], **Alice J. Lee**[1,3], **Ruth L. Stornetta**[1], and **J. Julius Zhu**[1,2]

[1]Department of Pharmacology, School of Medicine and College of Arts and Sciences, University of Virginia, Charlottesville, VA 22908

[2]Department of Neuroscience, School of Medicine and College of Arts and Sciences, University of Virginia, Charlottesville, VA 22908

[3]Department of Biology, School of Medicine and College of Arts and Sciences, University of Virginia, Charlottesville, VA 22908

Abstract

Deciphering interneuronal circuitry is central to understanding brain functions yet remains as a challenging task in neurobiology. Using simultaneous quadruple-octuple *in vitro* and dual *in vivo* whole-cell recordings, we found two previously unknown interneuronal circuits that link cortical layer 1–3 (L1-3) interneurons and L5 pyramidal neurons in the rat neocortex. L1 single-bouquet cells (SBCs) preferentially form unidirectional inhibitory connections on L2/3 interneurons that inhibit the entire dendritic-somato-axonal axis of ~1% of L5 pyramidal neurons located within the same column. In contrast, L1 elongated neurogliaform cells (ENGCs) frequently form mutual inhibitory and electric connections with L2/3 interneurons, and these L1-3 interneurons inhibit the distal apical dendrite of >60% of L5 pyramidal neurons across multiple columns. Functionally, SBC→L2/3 interneuron→L5 pyramidal neuronal circuits disinhibit and ENGC↔L2/3 interneuron→L5 pyramidal neuronal circuits inhibit the initiation of dendritic complex spikes in L5 pyramidal neurons. As dendritic complex spikes can serve coincidence detection, these cortical interneuronal circuits may be essential for salience selection.

INTRODUCTION

The cerebral cortex is capable of performing multifaceted high-level cognitive tasks, a capability believed to reside in the intricate cortical network that contains a diversity of cellular constituents, including a number of distinct inhibitory interneurons[1–6]. However, exactly how the cortical interneuronal circuits are structured to carry out cortical functions remains elusive due largely to the difficulty of deciphering complex neuronal circuits, a process requiring analysis of multi- or trans-synaptic connections and identification of cell types of many different interconnected interneurons and pyramidal neurons[7–9]. To facilitate the dissection of cortical interneuronal circuits, we developed a stable multiple (up to octuple) whole-cell recording technology that allows the recovery of the detailed

Address for correspondence: J. Julius Zhu, Department of Pharmacology, University of Virginia School of Medicine, 1300 Jefferson Park Avenue, Charlottesville, VA 22908, Tel: (434) 243-9246, Fax: (434) 982-3878, jjzhu@virginia.edu.
[4]These authors contribute equally.

AUTHOR CONTRIBUTIONS

X.J., G.W. and J.J.Z. designed and developed the mechanics (X.J. and J.J.Z.), electronics and software programs (G.W. and J.J.Z.) for the stable octuple whole-cell recording technology. X.J., G.W., R.L.S. and J.J.Z. developed the immunostaining, neuronal morphology and/or ultrastructural analysis procedures. X.J., G.W., A.J.L. and J.J.Z. performed the experiments and data analysis. X.J., G.W., A.J.L., R.L.S. and J.J.Z. wrote the manuscript.

COMPETING FINANCIAL INTERESTS

The authors declare no competing financial interests.

morphology of >85% of recorded interneurons and >99% of recorded pyramidal neurons. Using this technology, we were able to decode complex trans-synaptic interneuronal circuits in acute rat sensorimotor cortex slices.

Cortical layer 1 (**L1**) is likely involved in selection of attentional and salient signals because it receives inputs primarily from higher-order thalamic relays and higher-order cortical areas[10–13]. It has been demonstrated that neurons in these thalamic relays and cortical areas preferentially increase their activity during attention-demanding processes (e.g., attentional, expectational, perceptual and working memory tasks), and physiological or pharmacological manipulation of the activity of the neurons interferes with attentional tasks[14–17]. Strategically located in L1 are sparsely distributed GABAergic interneurons that belong to two general groups: one group of cells have a heterogeneous morphological appearance and an axon projecting to deeper layers, whereas the others are multipolar, aspiny neurons resembling neurogliaform cells (**NGCs**) with an axon ramifying densely within L1[18–21]. *In vivo* recordings show that L1 inputs generate direct, rapid excitatory postsynaptic potentials (**EPSPs**) in L1 interneurons, as well as in apical dendrites of pyramidal neurons in deep layers[19,22], and the excitation is selectively and dramatically enhanced during attentional tasks[23,24]. In L5 pyramidal neurons, near-synchronous L1 modulatory and L4 sensory inputs can serve as a coincidence detection mechanism by inducing dendritic complex spikes and bursts of somatic/axonal action potentials[22,25], which secure the further processing of the signals[26,27]. L1 interneurons can convert L1 inputs into inhibition to mold dendritic integration in pyramidal neurons[18–20,28,29]. However, whether L1 neurons may participate in more complex interneuronal circuits and what these circuits can do remains unclear.

Here we report two novel and distinct cortical interneuronal circuits that link input-receiving L1 interneurons via L2/3 interneurons to output-producing L5 pyramidal neurons in the rat sensorimotor cortex. One circuit involves a specific type of L1 neuron, the single-bouquet cells (**SBCs**), that typically formed unidirectional inhibitory connections with all seven types of L2/3 interneurons, and these L2/3 interneurons inhibited the entire dendritic-somato-axonal initial segment axis of a very small number of L5 pyramidal neurons located within the same column. Thus, SBC→L2/3 interneuron→L5 pyramidal neuronal circuits effectively enhanced dendritic complex spiking in L5 pyramidal neurons using a disynaptic disinhibitory mechanism. In contrast, the other circuit involves a different type of L1 neuron, the elongated neurogliaform cells (**ENGCs**), that frequently formed reciprocal inhibitory and electric connections with three selective types of L2/3 interneurons, and these L1 and L2/3 interneurons inhibited the distal apical dendrite of the majority of L5 pyramidal neurons in the same and neighboring columns. In this way ENGC↔L2/3 interneuron→L5 pyramidal neuronal circuits powerfully suppressed dendritic complex spiking in L5 pyramidal neurons using a mutual inhibition- and electric coupling-mediated synchronizing mechanism. Therefore, functioning beyond converting L1 inputs into inhibition, these two distinct interneuronal circuits could transform L1 inputs into complementary “filters” by differentially regulating the output of L5 pyramidal neurons such that together they may act synergistically to filter out “noise” in the incoming information and allow effective detection of salient signals.

RESULTS

We first studied L1-3 interneurons and interneuronal circuits using acute rat sensorimotor cortex slices. Inhibitory synaptic connections were identified by evoking unitary inhibitory postsynaptic currents (**uIPSCs**) or potentials (**uIPSPs**) with brief depolarizing current pulses (5 ms) applied in presynaptic neurons at 0.01–0.05 Hz in the presence of AMPA- and NMDA-receptor antagonists (20μM DNQX and 100 μM DL-APV). A total of 2,260

inhibitory connections were identified after testing 14,832 connections between 1,703 L1 neurons, 3,130 L2/3 interneurons, and/or 3,394 L5 pyramidal neurons in the cortical slices.

L1-3 interneurons form distinct circuits

Interneurons with very different patterns of axonal arborization were recorded in L1 (Fig. 1a,b; see also supplemental Movie S1). Anatomical analysis showed that many L1 neurons (n=466) had heterogeneous dendritic morphology and a characteristic vertically descending horsetail-like axonal bundle with short side branches similar to double-bouquet cells (**DBCs**) (Figs. 1a,b and S1a). However, they had few ascending axonal branches, more closely resembling bipolar cells (**BPCs**) than DBCs. The other neurons (n=196) resembled NGCs, but their axonal arborization was horizontally elongated compared to classic NGCs in other cortical layers (Figs. 1a,b and S1b). While the majority of deeper layer-projecting L1 neurons (n=439 out of 466) fired adapting non-late-spiking action potentials, the majority of NGC-like L1 neurons (n=175 out of 196) fired non-adapting late-spiking action potentials (Fig. 1a,c). These results are consistent with a recent suggestion that firing patterns can often (but not always) predict L1 interneuron cell types([21]; see also[18,19]). Thus, to avoid ambiguity, we classified L1 interneurons into two general groups using their distinct axonal arborization patterns. Following recently proposed nomenclature[4], we named these two groups of neurons as single bouquet/bundle cells (or **SBCs**) and elongated NGCs (or **ENGCs**), respectively.

We next investigated how SBCs and ENGCs connect with other neurons by examining their postsynaptic targets. Physiological recordings showed that both SBCs and ENGCs inhibited interneurons in L2/3. Independent of postsynaptic cell type, SBC-induced uIPSCs had shorter latencies, rise times and decay time constants compared to ENGC-induced uIPSCs (Figs. 2 and S2). Consistent with these results, SBC-induced uIPSPs were insensitive to the bath application of CGP35348, a $GABA_B$ receptor blocker, but were completely blocked by the bath application of PTX, a $GABA_A$ receptor blocker (Fig. S2). On the other hand, ENGC-induced uIPSPs were partially blocked by the bath application of CGP35348 and completely blocked by additional PTX in the bath solution (Fig. S2). These results indicate that SBC-induced uIPSPs are mediated primarily by $GABA_A$ receptors, whereas ENGC-induced uIPSPs are mediated by both $GABA_A$ and $GABA_B$ receptors.

Further analysis revealed that SBCs inhibited ~13% of L2/3 interneurons recorded in the same columns, but none of L2/3 interneurons recorded in neighboring columns (Fig. 3 and Table S1), suggesting that SBCs and L2/3 interneurons formed inhibitory circuits within single columns. In contrast, ENGCs inhibited ~20% of L2/3 interneurons recorded in the same columns and ~10% of those recorded in neighboring columns (Fig. 4 and Table S1), suggesting that ENGCs and L2/3 interneurons formed inhibitory circuits across multiple columns. Interestingly, SBCs rarely formed mutual inhibitory (~1%) and electric (0%) connections with L2/3 interneurons, while ENGCs frequently formed mutual inhibitory (~60%) and electric (~65% of whose with intersomatic distance <150 μm) connections with their postsynaptic L2/3 interneurons (Fig. S3 and Table S1). These results suggest that SBCs preferentially form unidirectional inhibitory connections with L2/3 interneurons, whereas ENGCs frequently form bidirectional inhibitory and/or electric connections with L2/3 interneurons.

Morphological reconstruction revealed that L2/3 interneurons had visibly distinct axonal arborization patterns (Fig. 5). To determine whether SBCs and ENGCs target different populations of L2/3 interneurons, we classified L2/3 interneurons into seven general types, including Martinotti cells (**MaCs**), NGCs, bitufted cells (**BTCs**), BPCs, basket cells (**BaCs**), DBCs and chandelier cells (**ChCs**) (Fig. 5a; see also supplemental Movie S2), using the axonal arborization-based interneuronal classification scheme[2,4]. Confirming the direct

visual assessment, axonal length density analysis indicated that these seven types of L2/3 interneurons differed significantly in their axonal arborization patterns (Fig. 5b and S1c–i). The classification and analysis suggested that SBCs inhibited all seven types of L2/3 interneurons we described, while ENGCs inhibited selectively MaCs, NGCs and BTCs (Table S1). Intriguingly, MaCs, NGCs and BTCs innervated by SBCs and ENGCs had similar axonal arborizations, but differed in somatodendritic properties (Fig. S4). In particular, MaCs, NGCs and BTCs postsynaptic to SBCs were located throughout the entire L2/3 with <10% of their dendritic arborization found in L1. In contrast, MaCs, NGCs and BTCs postsynaptic to ENGCs were located in the upper half of L2/3 with ~50% of their dendritic arborization positioned in L1 (Fig. S4). Collectively, these anatomical, physiological and pharmacological results indicate that SBCs and ENGCs form two anatomically and functionally distinct interneuronal circuits: SBC→ and ENGC↔L2/3 interneuronal circuits.

Interneuronal circuits differentially target L5 neurons

We then examined excitatory postsynaptic neurons targeted by SBC→ and ENGC↔L2/3 interneuronal circuits, focusing primarily on L5 pyramidal neurons, the major cortical output neurons (Figs. 3,4 and S5). Simultaneous whole-cell recordings from multiple L1-3 interneurons and L5 pyramidal neurons revealed that SBCs did not directly inhibit L5 pyramidal neurons (Figs. 3 and S5). Instead, L2/3 interneurons postsynaptic to SBCs inhibited ~9% of L5 pyramidal neurons located in the same columns, but these L2/3 interneurons did not inhibit L5 pyramidal neurons in neighboring columns (Figs. 3c,d and S5). In contrast, ENGCs directly inhibited ~20% of L5 pyramidal neurons recorded in the same columns and they also directly inhibited ~5% of L5 pyramidal neurons recorded in neighboring columns (Fig. 4). In addition, L2/3 interneurons postsynaptic to ENGCs inhibited ~20% of L5 pyramidal neurons in the same column (Figs. 4c,d and S5). Together, these results suggest that SBCs form disynaptic disinhibitory connections with L5 pyramidal neurons via L2/3 interneurons within single columns, whereas interconnected ENGCs and L2/3 interneurons form direct inhibitory connections with L5 pyramidal neurons in the same and/or neighboring columns.

To determine whether distinct L2/3 interneurons may be differentially involved in SBC→ and ENGC↔L2/3 interneuron→L5 pyramidal neuronal circuits, we further analyzed the inhibitory synaptic connections formed between distinct L2/3 interneurons and L5 pyramidal neurons. Interestingly, light microscopic examination suggested that each of seven types of L2/3 interneurons contacted a specific, largely non-overlapping subcellular compartment of L5 pyramidal neurons with multiple synaptic boutons, and together, they subdivided the entire membrane surface of the dendritic-somato-axonal initial segment region (Fig. 6 and Table S2). Specifically, the synaptic boutons of MaCs were on terminal tuft dendrites, those of NGCs were on secondary and tertiary tuft dendrites, those of BTCs were on distal dendritic trunks and primary tuft dendrites, those of BPCs were on middle dendritic trunks and oblique dendrites, those of BaCs were on somata and proximal dendrites, those of DBCs were on middle and distal basal dendrites, and those of ChCs were on axonal initial segments of L5 pyramidal neurons. At times, we recorded two (n=16) or three (n=4) distinct L2/3 interneurons innervating the same postsynaptic L5 pyramidal neurons, and morphological reconstruction showed that the synapses from distinct L2/3 interneurons did not intermingle in their target areas of L5 pyramidal neurons (Fig. 6a,b). Subsequent electron microscopic serial section examination confirmed that the majority of light microscopically identified synaptic boutons were actual synapses (~80%; n=69 of 89 boutons from 15 interneurons) with symmetric membrane densities (Fig. S6 and Table S2), consistent with the notion that light microscopically identified synaptic boutons are reliable indicators of synapses[30,31]. Collectively, these results suggest that L1-3 interneurons form

distinct interneuronal circuits, i.e., SBC→ and ENGC↔L2/3 interneuron→L5 pyramidal neuronal circuits differentially control distinct subcellular compartments of L5 pyramidal neurons.

Interneuronal circuits regulate dendritic complex spiking

To determine the possible functional roles of SBC→ and ENGC↔L2/3 interneuron→L5 pyramidal neuronal circuits, which seem to target multiple distinct dendritic-somato-axonal compartments in L5 pyramidal neurons[27,32–34], we examined their effects on dendritic and somatic spiking (Fig. 7). As with previous reports[22,25], simultaneously injecting currents in the shape of an EPSP at the dendrite and soma of L5 pyramidal neurons could evoke a dendritic complex spike and a burst of 2–3 somatic action potentials in the neurons (Fig. 7b,e). The dendritic complex spikes consisted of a sequence of events, including initially a soma/axon-initiated back-propagating action potential, then a dendrite-initiated slow action potential, and finally an additional one or more soma/axon-initiated action potential(s) (Fig. 7b inserts), indicative of the interplay of somatic/axonal and dendritic action potential zones[25]. Depolarizing L2/3 interneurons in either SBC→ or ENGC↔L2/3 interneuron→L5 pyramidal neuronal circuits with continuous current injection elicited tonic firing of single action potentials in interneurons, which induced uIPSPs in the dendrite and soma of L5 pyramidal neurons, and suppressed complex dendritic spiking and somatic bursting in L5 pyramidal neurons (Fig. 7c,e), consistent with previous findings[25]. Remarkably, action potentials in SBCs evoked by short depolarizing pulses effectively abolished the depolarization-elicited firing in all L2/3 interneurons, blocked L2/3 interneuron-mediated uIPSPs, and reversed the suppression of complex dendritic spiking and somatic bursting in L5 pyramidal neurons (n=9; Fig. 7d,e). There was a slight increase in incidence of dendritic complex spikes after current injection in both SBCs and their postsynaptic L2/3 interneurons (Fig. 7e), suggestive of the existence of additional L2/3 interneurons of the same disynaptic circuits located likely within the same compact columnar areas (Fig. 3). In sharp contrast, short pulse-evoked action potentials in ENGCs consistently synchronized the depolarization-elicited tonic firing in all L2/3 interneurons, potentiated L2/3 interneuron-mediated uIPSPs, and enhanced the suppression of complex dendritic spiking and somatic bursting in L5 pyramidal neurons (n=10; Fig. 7d,e). These results suggest that activation of SBC→L2/3 interneuronal circuits disinhibits and activation of ENGC↔L2/3 interneuronal circuits inhibits the initiation of complex dendritic spikes in L5 pyramidal neurons.

To confirm the functions of SBC→ and ENGC↔L2/3 interneuron→L5 pyramidal neuronal circuits in intact brains, we made simultaneous dual recordings from SBCs or ENGCs and L5 pyramidal neurons *in vivo* (Fig. 8). Simultaneous somatic recordings from SBCs and dendritic recordings from L5 pyramidal neurons showed numerous spontaneous or whisker-evoked events, which occasionally reached threshold and triggered somatic action potentials in SBCs and dendritic complex spikes in L5 pyramidal neurons. Correlation analysis revealed that in some paired recordings (n=3 out of 18 pairs) initiation of action potentials in SBCs enhanced dendritic complex spiking in L5 pyramidal neurons for ~200 ms (Fig. 8a,e). To confirm the causal effect, we elicited action potentials in SBCs by directly injecting short depolarizing pulses. The evoked action potentials in SBCs enhanced dendritic complex spiking in L5 pyramidal neurons in the same three paired recordings (Fig. 8c,e). Consistent with the *in vitro* results, the evoked action potentials in SBCs did not induce uIPSP in L5 pyramidal neurons (n=0 out of 18 pairs; Fig. 8c,d). Similarly, paired recordings showed that spontaneous or whisker-evoked events sometimes reached threshold and triggered somatic action potentials in ENGCs and dendritic complex spikes in L5 pyramidal neurons. However, in the majority of paired recordings (n=7 out of 8 pairs), spontaneous and whisker-evoked action potentials in ENGCs suppressed dendritic complex spiking in L5 pyramidal neurons for ~400 ms (Fig. 8b,e). In the same seven paired recordings, the short

pulse-evoked action potentials in ENGCs induced uIPSPs and blocked dendritic complex spiking in L5 pyramidal neurons (Fig. 8c,e), suggesting a direct causal effect. Interestingly, recordings from many ENGCs, but none of the SBCs, displayed spikelet-like events, some of which seemed involved in the initiation of action potentials in ENGCs (Fig. S7), suggesting a contribution of electric synapses in synchronizing firing in ENGC↔L2/3 interneuronal circuits. Collectively, these *in vitro* and *in vivo* results suggest that SBC→L2/3 interneuron→L5 pyramidal neuronal circuits serve to disinhibit, and in a complementary fashion, ENGC↔L2/3interneuron→L5 pyramidal neuronal circuits function to inhibit dendritic complex spiking in L5 pyramidal neurons.

DISCUSSION

In this study, we have deciphered the architecture of two novel interneuronal circuits that link L1-3 interneurons and L5 pyramidal neurons in the neocortex (Fig. S8). L1 SBCs preferentially form unidirectional inhibitory connections with all seven types of L2/3 interneurons and trans-synaptically control inhibition along the entire dendritic-somato-axonal axis of a few L5 pyramidal neurons within single columns. In contrast, L1 ENGCs frequently form mutual inhibitory and electric connections with only three selective types of L2/3 interneurons and they together regulate inhibition at the distal apical dendrite of many pyramidal neurons across multiple columns. Functionally, SBC→L2/3 interneuron→L5 pyramidal neuronal circuits disinhibit and ENGC↔L2/3 interneuron→L5 pyramidal neuronal circuits inhibit the initiation of dendritic complex spikes in L5 pyramidal neurons. Given that dendritic complex spiking can serve as a coincidence detection mechanism[22,25], these two interneuronal circuits may play a key role in selecting and processing salient information.

Organization of cortical interneuronal circuits

We report here two novel cortical interneuronal circuits, SBC→ and ENGC↔L2/3 interneurons→L5 pyramidal neuronal circuits, which exhibit distinct architecture (Fig. S8). Previous *in vitro* and *in vivo* recordings suggest that L1 SBCs fire adapting non-late-spiking action potentials whereas L1 ENGCs fire non-adapting late-spiking action potentials[18,19]. However, a recent study reports a few exceptions[21]. In this study, we have analyzed a large number of L1 interneurons and confirmed that there are actually many exceptions. Therefore, instead of relying on firing patterns, we classified L1 interneurons based on their visually distinguishable axonal arborization patterns, which are quantitatively confirmed with the axonal length density analysis (Fig. 1b), as well as Sholl and polar analyses (not shown). Importantly, SBCs preferentially form unidirectional inhibitory circuits with L2/3 interneurons and they produce $GABA_A$-R-mediated fast inhibition, while ENGCs frequently form mutual inhibitory and electric circuits with L2/3 interneurons and they generate $GABA_A$-R- and $GABA_B$-R-mediated slow inhibition.

SBC→ and ENGC↔L2/3 interneuronal circuits further differ in how they connect with L5 pyramidal neurons (Fig. S8). L5 pyramidal neurons have two general input-receiving domains, an apical dendritic domain and an oblique/basal dendritic-somato-axonal domain[22,33,35], which receive primarily modulatory and sensory inputs, respectively[13]. Our analysis reveals that seven types of L2/3 interneurons (i.e., MaCs, NGCs, BTCs, BPCs, BaCs, DBCs and ChCs) synapse on different subcellular compartments of L5 pyramidal neurons, and together their synapses subdivide the entire membrane surface of the dendritic-somato-axonal initial segment region. SBCs control both the apical and oblique/basal dendritic domains of L5 pyramidal neurons via inhibition of all seven types of L2/3 interneurons (Figs. 3 and 7), whereas ENGCs regulate only the apical dendritic domain of L5 pyramidal neurons via direct inhibition (Figs. 4 and 7) or via output synchronization with MaCs, NGCs and BTCs (Fig. 7). In particular, SBCs never inhibit L5 pyramidal neurons.

Instead, SBCs inhibit 13.0% of L2/3 interneurons, and these L2/3 interneurons inhibit 8.7% of L5 pyramidal neurons in the same columns (Figs. 3 and S5). Thus, we estimate that SBC→L2/3 interneuron→L5 pyramidal neuronal circuits may provide disinhibition on dendritic complex spiking in a small percentage (P = 13.0% • 8.7%≈1%) of disynaptically connected L5 pyramidal neurons. In contrast, ENGCs inhibit 20.4%, and MaC, NGC and BTC L2/3 interneurons postsynaptic to ENGCs inhibit 7.1%, 33.3% and 15.8% of L5 pyramidal neurons in the same columns (Fig. S5). These L1-3 interneurons may fire alone and independently inhibit L5 pyramidal neurons. Alternatively, when activated together they may fire in synchrony and thus more effectively inhibit L5 pyramidal neurons (Fig. 7). The synchronization of outputs in these interneurons seems dependent on their frequent mutual inhibitory and electrical synapses because these synapses can cooperate (complementarily and synergistically) in synchronizing firing in interneuronal networks; whereas electric gap junctional potentials (or spikelets) promote co-initiation of action potentials when inhibition fades (thus acting as an excitatory force), inhibitory synaptic potentials rapidly curtail spikelets and suppress initiation of action potentials during their presence (acting as an inhibitory force)[3,36,37]. Therefore, we calculate that ENGC↔L2/3 interneuron→L5 pyramidal neuronal circuits may inhibit the majority (P = 100% - (100%-20.4%) • (100%-7.1%) • (100%-33.3%) • (100%-15.8%)≈60%) of monosynaptically connected L5 pyramidal neurons located in the same columns alone. Together, these results suggest that SBC→L2/3 interneuron→L5 pyramidal neuronal circuits are structured to disinhibit a small population of L5 pyramidal neurons whereas ENGC↔L2/3 interneuron→L5 pyramidal neuronal circuits are organized to inhibit a large population of L5 pyramidal neurons.

Functional implications of cortical interneuronal circuits

Our results indicate that SBC→and ENGC↔L2/3 interneuron→L5 pyramidal neuronal circuits function beyond transforming L1 inputs into inhibition. Instead of suppressing, SBCs *enhance* dendritic complex spiking in L5 pyramidal neurons, via inhibiting L2/3 interneurons that are spontaneously active in intact brains[24,28,38,39]. Thus, SBC→L2/3 interneuron→L5 pyramidal neuronal circuits use a disynaptic disinhibitory mechanism to permit the initiation of dendritic complex spikes in a few L5 pyramidal neurons within a small area, which non-linearly amplifies the selected signals. On the other hand, ENGC↔L2/3 interneuron→L5 pyramidal neuronal circuits employ a mutual inhibition- and electric coupling-mediated synchronizing mechanism to synchronize the firing of interneurons. These interneurons can then supply powerful inhibition to *suppress* dendritic complex spiking in many L5 pyramidal neurons over a broader area, which effectively increases the signal-to-noise ratio by reducing background noise and sharpens the receptive field by suppressing surrounding activity. Moreover, SBCs have a smaller receptive field with higher acuity than ENGCs[19], which may produce a much smaller supra-threshold field[40–42]. Finally, SBCs receive the earliest L1 inputs, and they are rapidly inactivated after their initial activation[19], due presumably to the inhibition from ENGCs[18,20], and from MaCs, NGCs and BTCs targeted by ENGCs (Table S1). Together, these results suggest that SBC→ and ENGC↔L2/3 interneuron→L5 pyramidal neuronal circuits may work together to select and non-linearly amplify a very few spatially and temporally defined signals.

In this study, a few other intriguing architectural features of SBC→and ENGC↔L2/3 interneuron→L5 pyramidal neuronal circuits have emerged that may be of functional significance as well. For example, SBCs innervate relatively fewer (<10%) MaCs, NGCs, BaCs and DBCs, but more BTCs (14.6%) and ChCs (17.3%), and many more BPCs (27.9%) (Table S1). While BTCs and ChCs target the dendritic and axonal action potential initiation zones, respectively, BPCs target the middle dendritic trunk critical for interaction of the dendritic and axonal action potential initiation zones in L5 pyramidal neurons[22,43]. Therefore, we speculate that SBC→L2/3 interneuronal circuits may be particularly effective

in controlling the initiation of dendritic complex spikes, which requires the interaction of dendritic and axonal action potentials[25,43]. In addition, although MaCs, NGCs and BTCs involved in different circuits have the same axonal anatomy, they differ in dendritic branching patterns. In particular, MaCs, NGCs and BTCs targeted by ENGCs have their dendrites ramifying extensively into L1 (Fig. S4), and they may receive direct L1 inputs[11], enabling them to directly convert L1 inputs into inhibition in L5 pyramidal neurons. These results also suggest that MaCs, NGCs and BTCs may be further divided into functional subgroups, which is in line with other evidence supporting the possibility of functionally subdividing L2/3 interneurons (i.e., BaCs and NGCs; see[44–46]). One obvious question that remains to be addressed is how distinct groups and/or subgroups of L2/3 interneurons may differentially contribute to cortical functions and whether they alter their activity coordinately and/or independently during different information processing tasks and behavioral states in unanesthetized animals (cf.[28,39,47]).

We propose here that SBC→and ENGC↔L2/3 interneuron→L5 pyramidal neuronal circuits may control the filtering of information, which is supported by several lines of evidence. First, SBC→ and ENGC↔L2/3 interneuron→L5 pyramidal neuronal circuits control the initiation of dendritic complex spikes, which can function as a coincidence detection mechanism to select salient inputs[22,25]. Second, the primary L1 inputs come from feed-forward connections from higher-order thalamic relays and feedback connections from higher-order cortical areas[10–13], and the neuronal activity in these thalamic relays and cortical areas initiates selection of salient information[14,15,17,48]. Third, theoretical and experimental studies suggest that attentional influence consists of both the signal augmenting and receptive field sharpening processes[15,17]. Consistent with this concept, SBC→L2/3 interneuronal circuits enhance dendritic complex spiking in a small spatially and temporally restricted population of L5 pyramidal neurons and ENGC↔L2/3 interneuronal circuits suppress dendritic complex spiking in the majority of L5 pyramidal neurons over a large area, effectively augmenting the signal-to-noise ratio and sharpening the receptive field. Finally, salience selection is central to many attention-demanding high-level cognitive behaviors, and accumulating evidence indicates a number of neurological, mental and/or psychiatric disorders associated with attention deficits exhibit impairments of interneuronal function (e.g., [15,49]).

ONLINE METHODS

Animal preparation

Young and adult male and female Sprague Dawley rats (≥postnatal 20-d-old), whose cortical inhibitory neurons and circuits are largely mature and relatively stabilized[49,51], were used for *in vitro* (p20–41 with ~90% of them to be p20–28; n=1,104) and *in vivo* (p27–70; n=172) experiments in this study. All procedures for animal surgery and maintenance were performed following protocols approved by the Animal Care & Use Committee of the University of Virginia and in accordance with US National Institutes of Health guidelines. For *in vitro* experiments, the sensorimotor cortical brain slice preparation followed our previous studies[22,52]. In brief, animals were deeply anesthetized by sodium pentobarbital (90 mg/kg) and decapitated. The brain was quickly removed and placed into cold (0–4°C) oxygenated physiological solution containing (in mM): 125 NaCl, 2.5 KCl, 1.25 NaH_2PO_4, 25 $NaHCO_3$, 1 $MgCl_2$, 25 dextrose, and 2 $CaCl_2$, pH 7.4. Parasagittal slices 350 μm thick were cut from the tissue blocks with a microslicer, at an angle (<~4°) closely parallel to apical dendrites of L5 pyramidal neurons, which retained the majority of distal ascending and descending axonal trees of L1-3 interneurons that project into L1 and L5–6. These slices were kept at 37.0±0.5°C in oxygenated physiological solution for ~0.5–1 hr before recordings. During the recording the slices were submerged in a chamber and stabilized with a fine nylon net attached to a platinum ring. The recording chamber was perfused with

oxygenated physiological solution containing additional AMPA- and NMDA-receptor antagonists 20 μM DNQX and 100 μM DL-APV. The half-time for the bath solution exchange was ~6 sec, and the temperature of the bath solution was maintained at 34.0±0.5°C. All antagonists were bath applied. For *in vivo* experiments, animals were initially anesthetized by an intraperitoneal injection of sodium pentobarbital (60 mg/kg) as previously reported[22,38,39]. Supplemental doses (10 mg/kg)of sodium pentobarbital were given as needed to keep animals free from pain reflexes and in a state of *light* slow-wave general anesthesia as determined by monitoring the cortical electroencephalogram(EEG), and a relatively steady membrane potential, which were ideal for observing dendritic complex spikes[19,22,38]. All pressure points and incised tissues are infiltrated with bupivacaine. Body temperature (rectal) was monitored and maintainedwithin 37.2±0.3°C.

Histology and electron microscopy

Light and electron microscopic (**LM** and **EM**) examinations were carried out following the procedures of our previous reports[22,53]. In brief, after *in vitro* recordings, the slices were fixed by immersion in 3% acrolein/4% paraformaldehyde in 0.1 M PBS at 4°C for 24 hrs, and then processed with the avidin-biotin-peroxidase method to reveal cell morphology. Some of the slices were subsequently sectioned into 60 μm sections, postfixed in 1% OsO_4, counterstained with 1% uranyl acetate, and flat embedded into resin to carry out EM examination. The morphologically recovered cells were examined, drawn and analyzed with the aid of a microscope equipped with a computerized reconstruction system Neurolucida (MicroBrightField, Colchester, VT). Axonal length density plots and maps were calculated per voxel (50 μm × 50 μm × 350 μm) using a custom-made program following a previous report[54]. The pyramidal neurons were normalized according to the soma and the main branch point of their apical dendrites (cf.[22]). For EM examination, the small areas of interest (~50 μm × ~50 μm), each containing putative synaptic boutons from single presynaptic neurons, were embedded in resin, carefully excised and resectioned into 80 nm serial ultrathin sections using an ultramicrotome. No excision and resection was made if synaptic boutons originated from different presynaptic neurons that were too close to be separated. The serial ultrathin sections were examined in sequence with a JEOL-1230 transmission electron microscope (Japan Electron Optic, Tokyo, Japan) following the labeled dendrites, which typically led to all LM-identified synapses (except a very few synapses destroyed during EM processing or hidden behind the grids) at the order predicted by Neurolucida reconstruction. Inhibitory synaptic contacts were determined based on the generally accepted criteria[55], including: 1) presence of membranes with parallel alignment forming synaptic clefts that are wider in the middle and close up at one or both edges; 2) absence of a prominent postsynaptic density; and 3) presence of multiple flattened synaptic vesicles with at least one docked at the presynaptic membrane.

Electrophysiology

Simultaneous whole-cell *in vitro* and *in vivo* recordings were obtained from cortical neurons as described previously[22,38,39,56]. Briefly, patch recording pipettes (4–7 MΩ) were filled with intracellular solutions containing (mM): 135 cesium methanesulfonate, 10 HEPES, 2.5 $MgCl_2$, 4 Na_2ATP, 0.4 Na_3GTP, 10 sodium phosphocreatine, 0.6 EGTA, 0.1 spermine and 0.5% biocytin, at pH 7.25 for current recordings, or 120 potassium gluconate, 10 HEPES, 4 KCl, 4 MgATP, 0.3 Na_3GTP, 10 sodium phosphocreatine and 0.5% biocytin, at pH 7.25, for voltage recordings. Whole-cell recordings were made with up to eight Axopatch 200B and/or Axoclamp 2A/B amplifiers (Molecular Devices, Sunnyvale, CA). To get a relatively unbiased population sample of each type of L2/3 interneuron in cortical slices, we randomly recorded all L2/3 neurons, except pyramidal neurons with an obvious apical dendrite. L5 pyramidal neurons were typically targeted after L1–2/3 interneuronal connections were established. As described in the previous reports[22,38,39], *in vivo* dual recordings were

targeted to neurons with the same receptive field. Dendritic recordings from L5 pyramidal neurons in intact brain were identified by their characteristic complex spikes, the recording sites were estimated from the distance that the micromanipulator had advanced, taking into account the angle that the electrode formed with the surface of the barrel cortex, and subsequently confirmed with the reconstructed electrode penetration pathways that were revealed after histology processing[38]. An ITC-18 interface board (HEKA Instruments Inc, Bellmore, NY) was custom-modified to achieve simultaneous A/D and D/A conversions of current, voltage, command and triggering signal for up to eight amplifiers. Custom-written Igor-based programs were used to operate the recording system and perform online and offline data analysis. Motorized manipulators (Lugis & Neumann Feinmechanik and Elektrotechnik, Ratingen, Germany) were custom-improved in stability to improve morphological recovery of axonal arborization of the recorded interneurons. More than 85% of recorded interneurons had their axonal arborization well-recovered and thus could be unambiguously classified into anatomical groups. These interneurons were included in the analysis. Neurons located in the same and neighboring columns were targeted by referring their relative locations to the barrels (if barrel cortical slices were used)[57], and/or more often to the characteristic clusters of ~10–20 closely packed large L5 pyramidal neurons located just inside of the columnar borders[52,58]. Since no difference was found in general interneuronal circuit organization between the sensory and motor cortices (Tables 3,4), the data were pooled in analysis. The presynaptic single action potential-evoked uIPSCs or uIPSPs in >3-week old cortical neurons are highly reliable and often show no transmission failure[59,60]. Thus, inhibitory synaptic connections could be unambiguously identified after online monitoring of the average responses of short latency uIPSPs for ≥50 episodes. Unless otherwise specified, IPSCs and IPSPs were measured with membrane potentials of postsynaptic cells clamped or held at −55 mV and −55 ± 3 mV, respectively. Recording traces shown were averages of 50–200 consecutive episodes and the averages were also used to calculate the basic properties and kinetics of evoked uIPSCs/uIPSPs, such as synaptic latency, 10–90% rise time and decay time constant. Since interneurons in acute slices seldom fired spontaneous action potentials, to achieve the maximal or near maximal suppression of dendritic complex spikes in L5 pyramidal neurons, we injected continuous depolarizing currents to induce tonic firing at ~5–15 Hz in L2/3 interneurons (Fig. 7). We then injected short depolarizing pulses at ~7–10 Hz in SBCs and ENGCs to evoke action potentials. The action potentials in SBCs blocked and those in ENGCs synchronized (to the same ~7–10 Hz) the firing in their connecting L2/3 interneurons (Fig. 7). Because the interaction of chemical and electric synapses is both necessary and effective in inducing stable firing synchronization in interneuronal networks[36,37], the mutual chemically and electrically connected ENGC and L2/3 interneuron pairs, the predominant connection configuration of the neurons (Fig. S3), were selected to carry out the experiment in figure 7.

Statistical analysis

Statistical results were reported as mean±s.e.m. The sample size (n) represents the number of neurons, unless otherwise indicated. Statistical significances of the means ($p \leq 0.05$; two sides) were determined using Wilcoxon and ANOVA, Mann-Whitney Rank Sum non-parametric or Chi-squared tests for paired and unpaired samples, respectively.

Supplementary Material

Refer to Web version on PubMed Central for supplementary material.

Acknowledgments

We thank Drs. Ed Callaway, Alev Erisir, Josh Huang, Jaideep Kapur and Gabor Tamas for technical advice and invaluable discussions, and members of the Zhu laboratory for comments and technical assistance. This study is

supported in part by a postdoctoral fellowship from the Epilepsy Foundation (X.L.), and a small research grant from the College of Arts and Sciences of the University of Virginia (A.L.) and NIH.

References

1. McBain CJ, Fisahn A. Interneurons unbound. Nature reviews. Neuroscience. 2001; 2:11–23.
2. Markram H, et al. Interneurons of the neocortical inhibitory system. Nature reviews. Neuroscience. 2004; 5:793–807.
3. Bartos M, Vida I, Jonas P. Synaptic mechanisms of synchronized gamma oscillations in inhibitory interneuron networks. Nature reviews. Neuroscience. 2007; 8:45–56.
4. Ascoli GA, et al. Petilla terminology: nomenclature of features of GABAergic interneurons of the cerebral cortex. Nature reviews. Neuroscience. 2008; 9:557–568.
5. Burkhalter A. Many specialists for suppressing cortical excitation. Frontiers in neuroscience. 2008; 2:155–167.10.3389/neuro.01.026.2008 [PubMed: 19225588]
6. Klausberger T, Somogyi P. Neuronal diversity and temporal dynamics: the unity of hippocampal circuit operations. Science. 2008; 321:53–57. [PubMed: 18599766]
7. Luo L, Callaway EM, Svoboda K. Genetic dissection of neural circuits. Neuron. 2008; 57:634–660. [PubMed: 18341986]
8. Brown SP, Hestrin S. Cell-type identity: a key to unlocking the function of neocortical circuits. Current opinion in neurobiology. 2009; 19:415–421. [PubMed: 19674891]
9. Wu GK, Tao HW, Zhang LI. From elementary synaptic circuits to information processing in primary auditory cortex. Neuroscience and biobehavioral reviews. 2011; 35:2094–2104. [PubMed: 21609731]
10. Cauller LJ, Clancy B, Connors BW. Backward cortical projections to primary somatosensory cortex in rats extend long horizontal axons in layer I. The Journal of comparative neurology. 1998; 390:297–310. [PubMed: 9453672]
11. Gonchar Y, Burkhalter A. Distinct GABAergic targets of feedforward and feedback connections between lower and higher areas of rat visual cortex. J Neurosci. 2003; 23:10904–10912. [PubMed: 14645486]
12. Rubio-Garrido P, Perez-de-Manzo F, Porrero C, Galazo MJ, Clasca F. Thalamic input to distal apical dendrites in neocortical layer 1 is massive and highly convergent. Cereb Cortex. 2009; 19:2380–2395.10.1093/cercor/bhn259 [PubMed: 19188274]
13. Petreanu L, Mao T, Sternson SM, Svoboda K. The subcellular organization of neocortical excitatory connections. Nature. 2009; 457:1142–1145. [PubMed: 19151697]
14. Robinson DL, Petersen SE. The pulvinar and visual salience. Trends in neurosciences. 1992; 15:127–132. [PubMed: 1374970]
15. Gilbert CD, Sigman M. Brain states: top-down influences in sensory processing. Neuron. 2007; 54:677–696.10.1016/j.neuron.2007.05.019 [PubMed: 17553419]
16. Baluch F, Itti L. Mechanisms of top-down attention. Trends in neurosciences. 2011; 34:210–224.10.1016/j.tins.2011.02.003 [PubMed: 21439656]
17. Purushothaman G, Marion R, Li K, Casagrande VA. Gating and control of primary visual cortex by pulvinar. Nature neuroscience. 2012; 15:905–912.10.1038/nn.3106
18. Chu Z, Galarreta M, Hestrin S. Synaptic interactions of late-spiking neocortical neurons in layer 1. J Neurosci. 2003; 23:96–102. [PubMed: 12514205]
19. Zhu Y, Zhu JJ. Rapid arrival and integration of ascending sensory information in layer 1 nonpyramidal neurons and tuft dendrites of layer 5 pyramidal neurons of the neocortex. J Neurosci. 2004; 24:1272–1279. [PubMed: 14960597]
20. Wozny C, Williams SR. Specificity of synaptic connectivity between layer 1 inhibitory interneurons and layer 2/3 pyramidal neurons in the rat neocortex. Cereb Cortex. 2011; 21:1818–1826.10.1093/cercor/bhq257 [PubMed: 21220765]
21. Kubota Y, et al. Selective coexpression of multiple chemical markers defines discrete populations of neocortical GABAergic neurons. Cereb Cortex. 2011; 21:1803–1817.10.1093/cercor/bhq252 [PubMed: 21220766]

22. Larkum ME, Zhu JJ. Signaling of layer 1 and whisker-evoked Ca^{2+} and Na^{+} action potentials in distal and terminal dendrites of rat neocortical pyramidal neurons in vitro and in vivo. J Neurosci. 2002; 22:6991–7005. [PubMed: 12177197]
23. Cauller LJ, Kulics AT. The neural basis of the behaviorally relevant N1 component of the somatosensory-evoked potential in SI cortex of awake monkeys: evidence that backward cortical projections signal conscious touch sensation. Experimental brain research. Experimentelle Hirnforschung. Experimentation cerebrale. 1991; 84:607–619. [PubMed: 1864331]
24. Letzkus JJ, et al. A disinhibitory microcircuit for associative fear learning in the auditory cortex. Nature. 2011; 480:331–335.10.1038/nature10674 [PubMed: 22158104]
25. Larkum ME, Zhu JJ, Sakmann B. A new cellular mechanism for coupling inputs arriving at different cortical layers. Nature. 1999; 398:338–341. [PubMed: 10192334]
26. Lisman JE. Bursts as a unit of neural information: making unreliable synapses reliable. Trends in neurosciences. 1997; 20:38–43. [PubMed: 9004418]
27. Sjostrom PJ, Rancz EA, Roth A, Hausser M. Dendritic excitability and synaptic plasticity. Physiol Rev. 2008; 88:769–840. [PubMed: 18391179]
28. Gentet LJ, et al. Unique functional properties of somatostatin-expressing GABAergic neurons in mouse barrel cortex. Nature neuroscience. 2012; 15:607–612.10.1038/nn.3051
29. Palmer LM, et al. The cellular basis of $GABA_B$-mediated interhemispheric inhibition. Science. 2012; 335:989–993. [PubMed: 22363012]
30. Markram H, Lubke J, Frotscher M, Roth A, Sakmann B. Physiology and anatomy of synaptic connections between thick tufted pyramidal neurones in the developing rat neocortex. J Physiol (Lond). 1997; 500:409–440. [PubMed: 9147328]
31. Tamas G, Lorincz A, Simon A, Szabadics J. Identified sources and targets of slow inhibition in the neocortex. Science. 2003; 299:1902–1905. [PubMed: 12649485]
32. Reyes A. Influence of dendritic conductances on the input-output properties of neurons. Annu Rev Neurosci. 2001; 24:653–675. [PubMed: 11520915]
33. Nevian T, Larkum ME, Polsky A, Schiller J. Properties of basal dendrites of layer 5 pyramidal neurons: a direct patch-clamp recording study. Nature neuroscience. 2007; 10:206–214.
34. Larkum ME, Nevian T. Synaptic clustering by dendritic signalling mechanisms. Current opinion in neurobiology. 2008; 18:321–331. [PubMed: 18804167]
35. Antic SD. Action potentials in basal and oblique dendrites of rat neocortical pyramidal neurons. The Journal of physiology. 2003; 550:35–50.10.1113/jphysiol.2002.033746 [PubMed: 12730348]
36. Tamas G, Buhl EH, Lorincz A, Somogyi P. Proximally targeted GABAergic synapses and gap junctions synchronize cortical interneurons. Nature neuroscience. 2000; 3:366–371.
37. Kopell N, Ermentrout B. Chemical and electrical synapses perform complementary roles in the synchronization of interneuronal networks. Proceedings of the National Academy of Sciences of the United States of America. 2004; 101:15482–15487.10.1073/pnas.0406343101 [PubMed: 15489269]
38. Zhu JJ, Connors BW. Intrinsic firing patterns and whisker-evoked synaptic responses of neurons in the rat barrel cortex. Journal of neurophysiology. 1999; 81:1171–1183. [PubMed: 10085344]
39. Zhu Y, Stornetta RL, Zhu JJ. Chandelier cells control excessive cortical excitation: characteristics of whisker-evoked synaptic responses of layer 2/3 nonpyramidal and pyramidal neurons. J Neurosci. 2004; 24:5101–5108. [PubMed: 15175379]
40. Anderson JS, Lampl I, Gillespie DC, Ferster D. The contribution of noise to contrast invariance of orientation tuning in cat visual cortex. Science. 2000; 290:1968–1972. [PubMed: 11110664]
41. Petersen CC, Hahn TT, Mehta M, Grinvald A, Sakmann B. Interaction of sensory responses with spontaneous depolarization in layer 2/3 barrel cortex. Proceedings of the National Academy of Sciences of the United States of America. 2003; 100:13638–13643. [PubMed: 14595013]
42. Sun YJ, et al. Fine-tuning of pre-balanced excitation and inhibition during auditory cortical development. Nature. 2010; 465:927–931. [PubMed: 20559386]
43. Larkum ME, Zhu JJ, Sakmann B. Dendritic mechanisms underlying the coupling of the dendritic with the axonal action potential initiation zone of adult rat layer 5 pyramidal neurons. The Journal of physiology. 2001; 533:447–466. [PubMed: 11389204]

44. Glickfeld LL, Scanziani M. Distinct timing in the activity of cannabinoid-sensitive and cannabinoid-insensitive basket cells. Nature neuroscience. 2006; 9:807–815.
45. Foldy C, Lee SY, Szabadics J, Neu A, Soltesz I. Cell type-specific gating of perisomatic inhibition by cholecystokinin. Nature neuroscience. 2007; 10:1128–1130.
46. Tricoire L, et al. Common origins of hippocampal Ivy and nitric oxide synthase expressing neurogliaform cells. J Neurosci. 2010; 30:2165–2176. [PubMed: 20147544]
47. Adesnik H, Bruns W, Taniguchi H, Huang ZJ, Scanziani M. A neural circuit for spatial summation in visual cortex. Nature. 2012; 490:226, 231.10.1038/nature11526 [PubMed: 23060193]
48. Corbetta M, Shulman GL. Control of goal-directed and stimulus-driven attention in the brain. Nature reviews. Neuroscience. 2002; 3:201–215.10.1038/nrn755
49. Batista-Brito R, Fishell G. The developmental integration of cortical interneurons into a functional network. Curr Top Dev Biol. 2009; 87:81–118. [PubMed: 19427517]
50. Perez-Garci E, Gassmann M, Bettler B, Larkum ME. The $GABA_{B1b}$ isoform mediates long-lasting inhibition of dendritic Ca^{2+} spikes in layer 5 somatosensory pyramidal neurons. Neuron. 2006; 50:603–616. [PubMed: 16701210]
51. Huang ZJ, Di Cristo G, Ango F. Development of GABA innervation in the cerebral and cerebellar cortices. Nature reviews. Neuroscience. 2007; 8:673–686.
52. Zhu JJ. Maturation of layer 5 neocortical pyramidal neurons: amplifying salient layer 1 and layer 4 inputs by Ca^{2+} action potentials in adult rat tuft dendrites. J Physiol (Lond). 2000; 526:571–587. [PubMed: 10922009]
53. Kielland A, et al. Activity patterns govern synapse-specific AMPA-R trafficking between deliverable and synaptic pools. Neuron. 2009; 62:84–101. [PubMed: 19376069]
54. Shepherd GM, Stepanyants A, Bureau I, Chklovskii D, Svoboda K. Geometric and functional organization of cortical circuits. Nature neuroscience. 2005; 8:782–790.
55. Peters, A.; Palay, SL.; Webster, Hd. The fine structure of the nervous system: neurons and their supporting cells. 3. Oxford University Press; 1991.
56. Margrie TW, Brecht M, Sakmann B. In vivo, low-resistance, whole-cell recordings from neurons in the anaesthetized and awake mammalian brain. Pflugers Archiv: European journal of physiology. 2002; 444:491–498. [PubMed: 12136268]
57. Agmon A, Connors BW. Thalamocortical responses of mouse somatosensory (barrel) cortex in vitro. Neuroscience. 1991; 41:365–379. [PubMed: 1870696]
58. Ito M. Simultaneous visualization of cortical barrels and horseradish peroxidase-injected layer 5b vibrissa neurones in the rat. The Journal of physiology. 1992; 454:247–265. [PubMed: 1282157]
59. Tamas G, Szabadics J, Somogyi P. Cell type- and subcellular position-dependent summation of unitary postsynaptic potentials in neocortical neurons. J Neurosci. 2002; 22:740–747. [PubMed: 11826103]
60. Szabadics J, Tamas G, Soltesz I. Different transmitter transients underlie presynaptic cell type specificity of $GABA_{A,slow}$ and $GABA_{A,fast}$. Proceedings of the National Academy of Sciences of the United States of America. 2007; 104:14831–14836. [PubMed: 17785408]

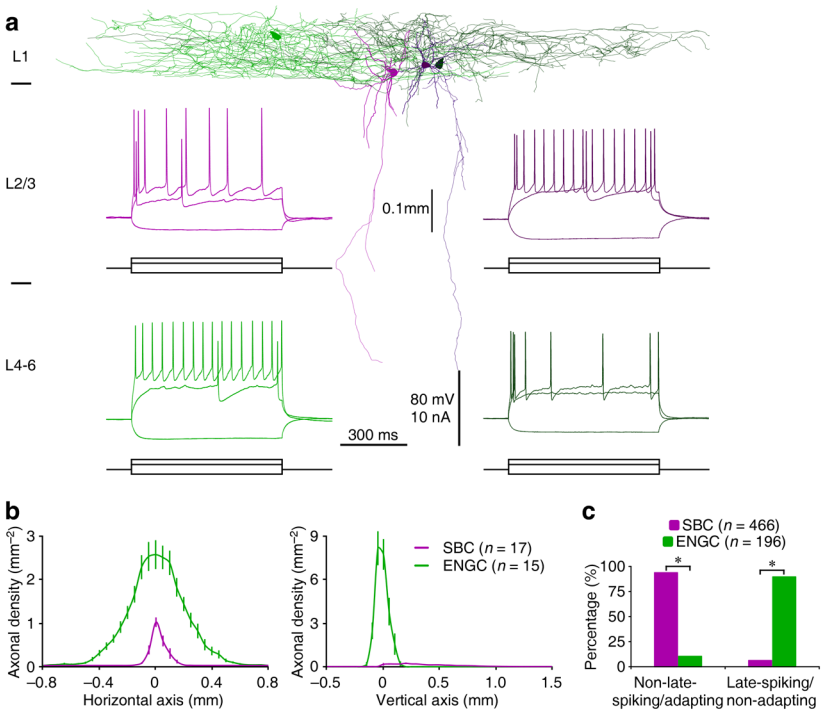

Fig. 1. L1 interneurons SBCs and ENGCs differ in preferential spiking patterns

(a) Reconstruction of two SBCs (pink and dark pink) and two ENGCs (green and dark green) recorded in L1 from acute cortical slices. Note the deeper layer-projecting axons from SBCs and largely L1-restricted axons from ENGCs. Inserted recordings show that one SBC fired typical adapting non-late-spiking (upper left) and the other SBC fired non-adapting late-spiking (upper right), and one ENGC fired typical nonadapting late-spiking (lower left) and the other ENGC fired adapting non-late-spiking (lower right) in response to near- and supra-threshold current injections. Scale bars apply to all recording traces.

(b) Axonal length density plots of L1 neurons (SBC: n=17; ENGC: n=15; F=318.9; p<0.001; ANOVA tests). Note the origin of X and Y axes indicating the soma location of interneurons and the positive direction of the vertical axis pointing to the cortical white matter.

(c) Histograms indicate that the majority of SBCs displayed adapting non-late-spiking firing pattern (SBC: 94.2%, n=439 of 466 tested; ENGC: 10.7%, n=21 of 196 tested; χ^2=456.2) whereas the majority of ENGCs displayed non-adapting late-spiking firing pattern (SBC: 5.8%, n=27 of 466 tested; ENGC: 89.3%, n=175 of 196 tested; χ^2=456.2). Asterisks indicate p<0.0005 (Chi-squared tests).

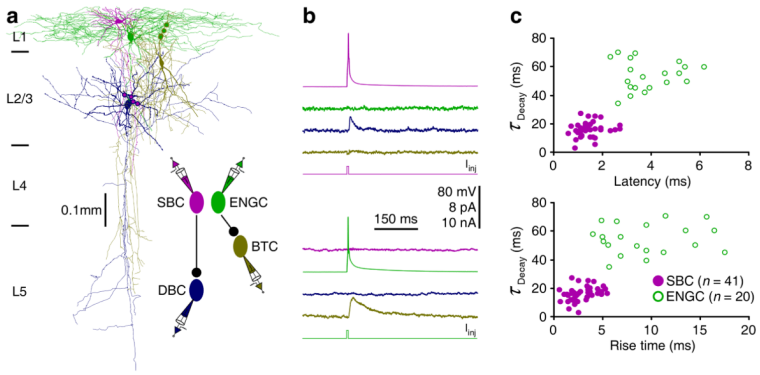

Fig. 2. L1-3 interneurons form two distinct inhibitory circuits

(a) Reconstruction of L1 SBC (pink), L1 ENGC (green), L2/3 DBC (blue) and L2/3 BTC (yellow) recorded simultaneously from an acute cortical slice. The double colored dots indicate the putative synaptic contacts. The schematic drawing shows symbolically the synaptic connections.

(b) Single action potentials elicited in SBC and ENGC evoked uIPSCs in postsynaptic DBC and BTC, respectively. Scale bars apply to all recording traces with 8 pA and 10 nA bars applied to uIPSC and current injection traces, respectively.

(c) Plots of the latencies and rise times against decay time constants of SBC- and ENGC-induced uIPSCs in L2/3 interneurons show significant differences in kinetics (Mann-Whitney Rank Sum tests). Values for the latencies (SBC: 1.4±0.1 ms, n=41; ENGC: 3.8±0.3 ms, n=20; U=7.5; p<0.001), rise times (SBC: 3.4±0.2 ms, n=41; ENGC: 9.9±0.9 ms, n=20; U=25; p<0.001), and decay time constants (SBC: 15.7±0.8 ms, n=41; ENGC: 54.8±3.0 ms, n=20; U=31; p<0.05) of SBC- and ENGC-induced uIPSCs.

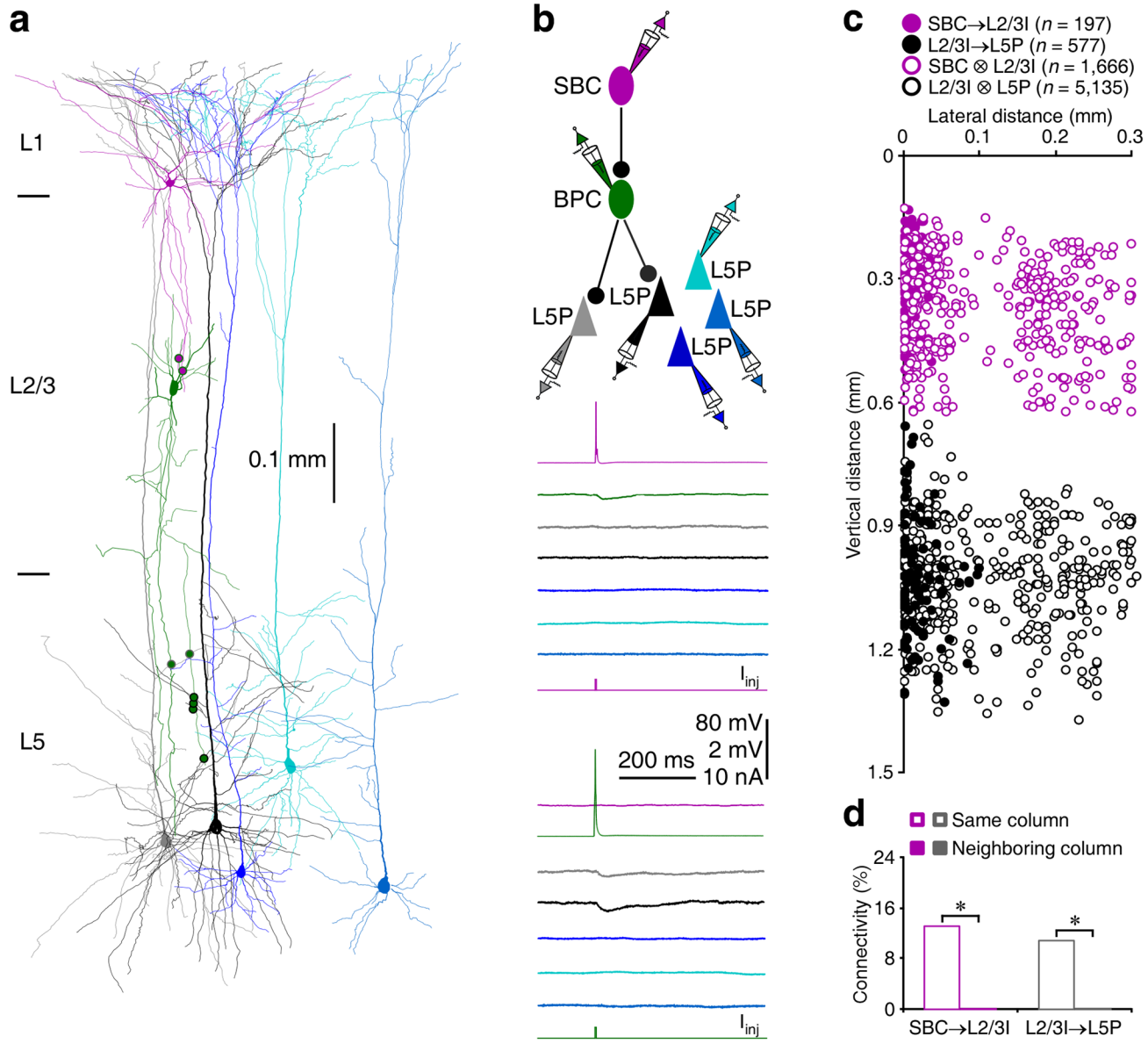

Fig. 3. SBCs form inhibitory circuits within single columns

(a) Reconstruction of L1 SBC (pink), L2/3 BPC (dark green), and multiple L5 pyramidal neurons recorded simultaneously from an acute cortical slice. The double colored dots indicate the putative synaptic contacts.

(b) Single action potentials elicited in presynaptic SBC and BPC evoked uIPSPs in postsynaptic BPC and two L5 pyramidal neurons (grey and black), respectively. The above schematic drawing shows symbolically the synaptic connections. Scale bars apply to all recording traces with 80 mV and 2 mV bars applied to traces with and without action potentials, respectively.

(c) The plot shows the relative position of L2/3 interneurons and L5 pyramidal neurons to SBCs and connectivity between SBCs and L2/3 interneurons or L2/3 interneurons and L5 pyramidal neurons in the same and neighboring columns. Note the origin of X and Y axes

indicating the soma location of SBCs, filled and empty dots representing connected and unconnected neurons, respectively, and reduced cell density at the border of columns. **(d)** Values for the connectivity of SBC→L2/3I (SBC→$L2/3I_{Same\ column}$: 13.0%, n=197 of 1,510 tested connections; SBC→$L2/3I_{Neighboring\ column}$: 0.0%, n=0 of 353 tested connections;χ^2=51.5) and L2/3I→L5P (L2/3I→$L5P_{Same\ column}$: 10.8%, n=577 of 5,330 tested connections; L2/3I→$L5P_{Neighboring\ column}$: 0.0%, n=0 of 382 tested connections; χ^2=46.0). Asterisks indicate p<0.05 (Chi-squared tests).

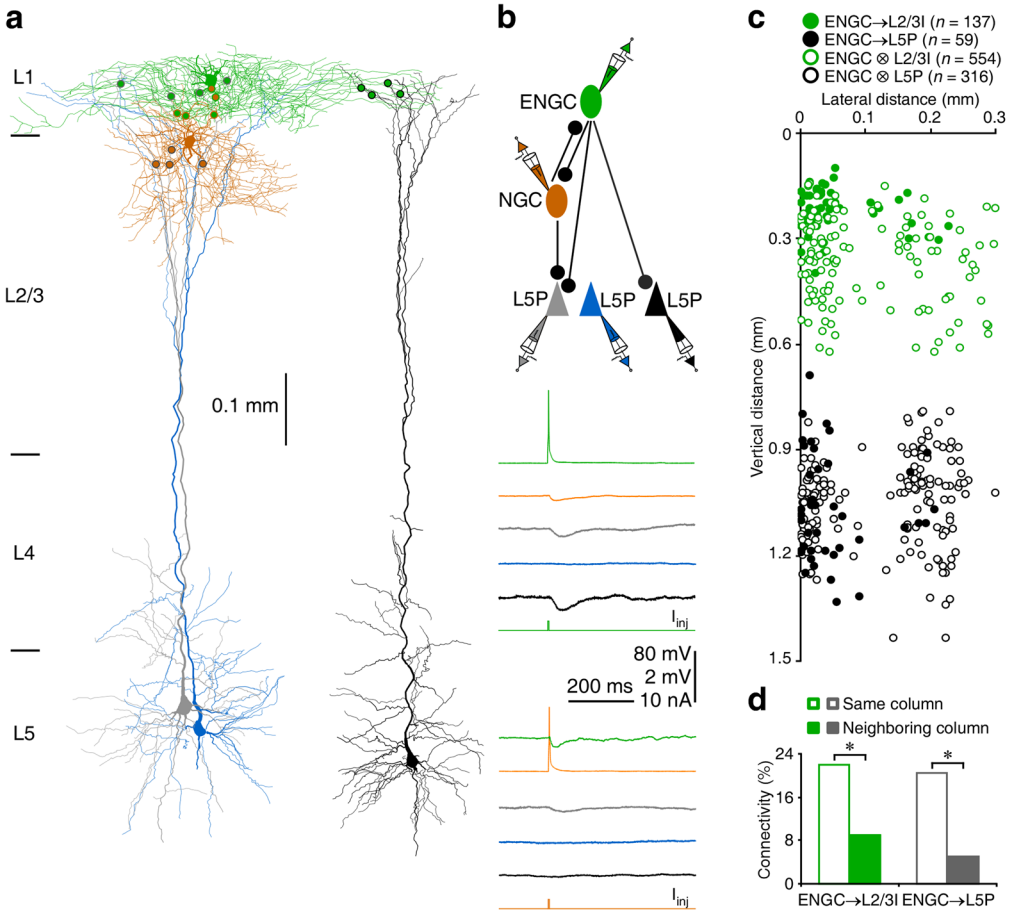

Fig. 4. ENGCs form inhibitory circuits across multiple columns

(a) Reconstruction of L1 ENGC (green), L2 NGC (brown) and multiple L5 pyramidal neurons recorded simultaneously. The double colored dots indicate the putative synaptic contacts. Note the putative synaptic contacts from ENGC on terminal tuft dendrites of L5 pyramidal neurons.

(b) Single action potentials elicited in presynaptic ENGC and NGC evoked uIPSPs in postsynaptic NGC, ENGC and two L5 pyramidal neurons (grey and black). The above schematic drawing shows symbolically the synaptic connections. Scale bars apply to all recording traces with 80 mV and 2 mV bars applied to traces with and without action potentials, respectively.

(c) The plot shows the relative position of L2/3 interneurons and L5 pyramidal neurons to ENGCs and connectivity between ENGCs and L2/3 interneurons or L5 pyramidal neurons in the same and neighboring columns. Note the origin of X and Y axes indicating the soma location of ENGCs, filled and empty dots representing connected and unconnected neurons, respectively, and reduced cell density at the border of columns.

(d) Values for the connectivity of ENGC→L2/3I (ENGC→$L2/3I_{Same\ column}$: 22.1%, n=126 of 570 tested connections; ENGC→$L2/3I_{Neighboring\ column}$: 9.1 %, n=11 of 121 tested connections; χ^2=10.6) and ENGC→L5P (ENGC→$L5P_{Same\ column}$: 20.4%, n=53 of 259 tested connections; ENGC→$L5P_{Neighboring\ column}$: 5.2%, n=6 of 116 tested connections; χ^2=14.1). Asterisks indicate p<0.05 (Chi-squared tests).

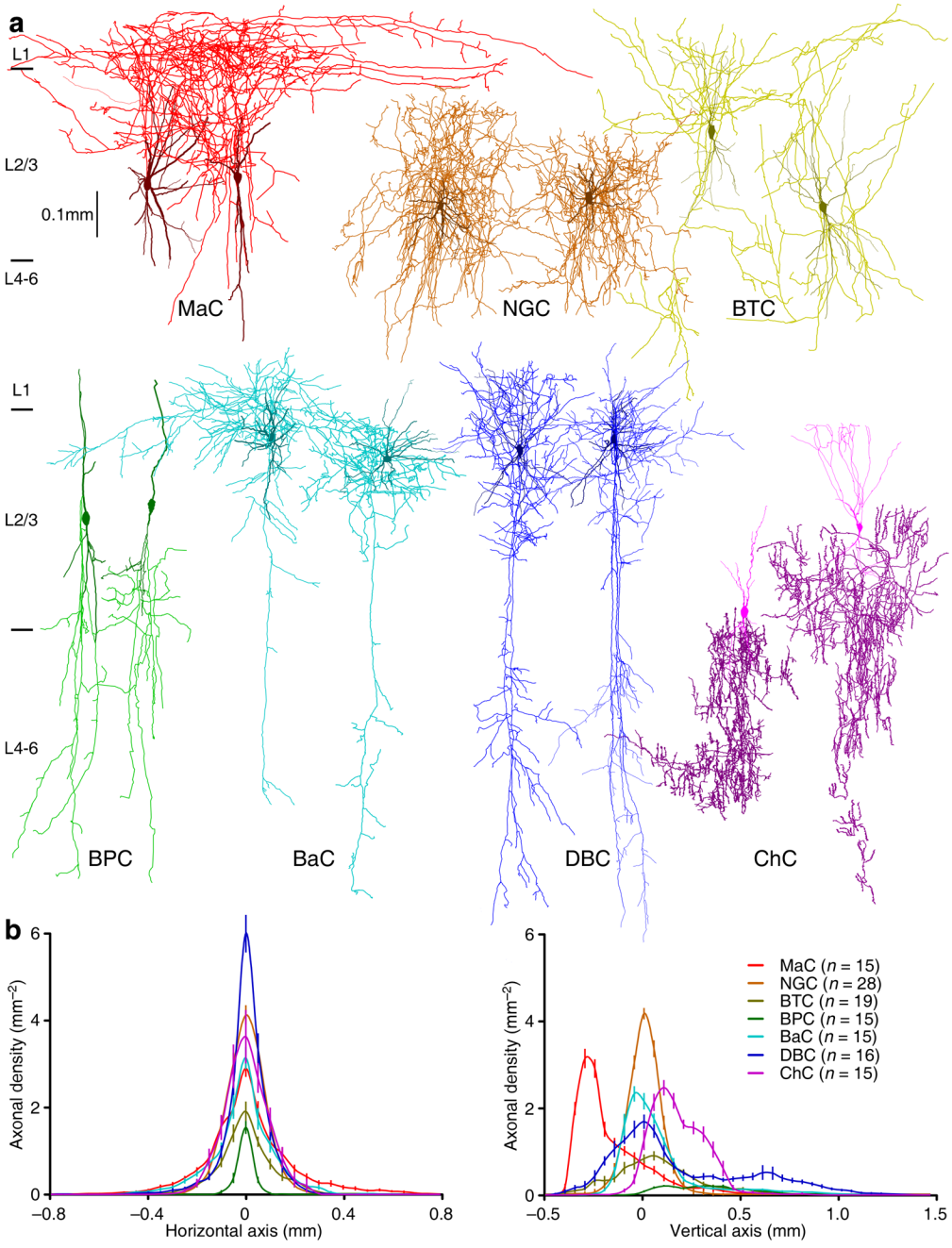

Fig. 5. L2/3 interneurons exhibit distinctive axonal arborization patterns

(a) Reconstruction of two MaCs (red), two NGCs (brown), two BTCs (yellow), two BPCs (dark green), two BaCs (cyan), two DBCs (blue) and two ChCs (purple) recorded in L2/3 of acute cortical slices.

(b) Axonal length density plots show significant differences in axonal density at both the horizontal and vertical axes of L2/3 interneurons (MaC: n=15; NGC: n=28; BTCs: n=19; BPC: n=15; BaC: n=15; DBC: n=16; ChC: n=15; F>185; p<0.001; ANOVA tests). Note the origin of X and Y axes indicating the soma location of interneurons and positive direction of the vertical axis pointing to the cortical white matter.

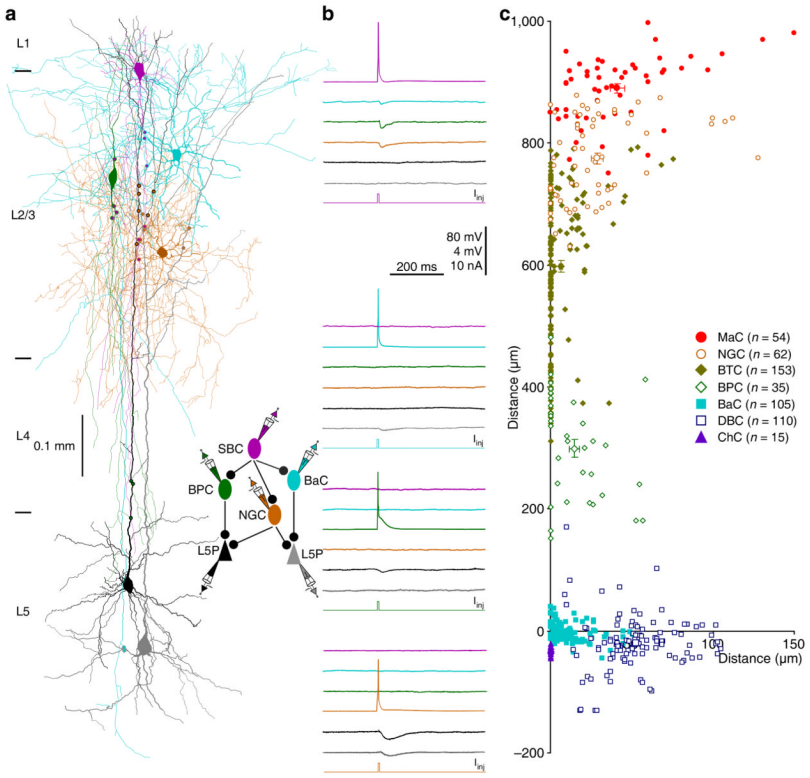

Fig. 6. L2/3 interneurons target different compartments of L5 pyramidal neurons

(a) Reconstruction of L1 SBC (pink), L2/3 NGC (brown), L2/3 BPC (dark green), L2/3 BaC (cyan) and two L5 pyramidal neurons (black and gray) recorded simultaneously from an acute cortical slice. The double colored dots indicate the putative synaptic contacts.

(b) Single action potentials elicited in presynaptic SBC, NGC, BPC and BaC evoked uIPSPs in postsynaptic NGC, BPC, BaC and L5 pyramidal neurons, respectively. The above schematic drawing shows symbolically the synaptic connections. Scale bars apply to all recording traces with 80 mV and 4 mV bars applied to traces with and without action potentials, respectively.

(c) The coordinates, or the horizontal and vertical distance of the synapses made by seven groups of L2/3 interneurons from the soma of L5 pyramidal neurons (MaC: lateral=41.2±4.3μm, vertical=890.3±7.4 μm; n=54 from 10 MaCs; NGC: lateral=28.8±3.8μm, vertical=774.3±8.6μm; n=62 from 17 NGCs; BTC: lateral=6.5±1.1μm, vertical=597.3±9.9μm; n=153 from 27 BTCs; BPC: lateral=14.5±3.2μm, vertical=299.5±14.4μm; n=35 from 8 BPCs; BaC: lateral=11.8±1.2μm, vertical= −0.6±1.5μm; n=105 from 28 BaCs; DBC: lateral=53.0±2.2μm, vertical=−19.2±4.3μm; n=110 from 26 DBCs; ChC: lateral=0.0±0.0 μm, vertical=−30.6±1.6μm; n=15 from 4 ChCs). The coordinates not shown (MaC$_{\leftarrow ENGC}$: lateral=41.6±7.5μm, vertical=898.2±8.3μm; n=14 from 3 MaCs; NGC$_{\leftarrow ENGC}$: lateral=32.1±5.3μm, vertical=783.6±11.5μm; n=38 from 11 NGCs; BTC$_{\leftarrow ENGC}$: lateral=8.0±1.8μm, vertical=601.8±24.0μm; n=38 from 7 BTCs; ENGC: lateral=70.8±7.6 μm, vertical=937.2±5.1 μm; n=27 from 6 ENGCs).

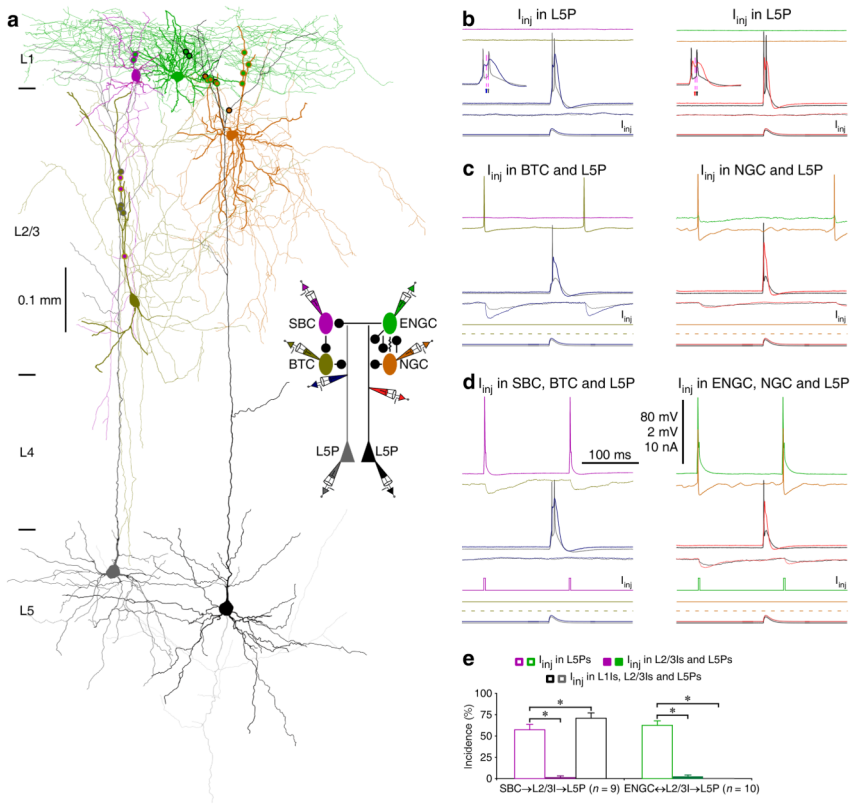

Fig. 7. SBC→ and ENGC↔L2/3I→L5 pyramidal neuronal circuits serve different functions

(a) Reconstruction of L1-3 interneurons and L5 pyramidal neurons recorded simultaneously from an acute cortical slice. The double colored dots indicate the putative synaptic contacts. The schematic drawing shows symbolically the synaptic connections and dendritic recording sites.

(b–d) The effects of continuous (in L1 interneurons) or brief (in L2/3 interneurons) depolarizing current injections on the complex dendritic complex spikes evoked by simultaneous near-threshold current injections from the dendritic and somatic recording electrodes in the shape of an EPSP. Scale bars apply to all recording traces in **b**–**d** with 80 mV and 2 mV bars applied to traces with and without action potentials, respectively. Note the reduced number of somatic action potentials after activation of L2/3 interneurons (N_{Before}: 2.3±0.1; N_{After}: 1.0±0.0, n=19;Z=4.0; p<0.005; Wilcoxon test) and NGC firing-evoked spikelets in ENGC.

(e) The incidences of dendritic complex spikes after current injections in L1-3 interneurons. Values for the incidences in SBC (I_{inj} in L5P: 56.9±6.6%; I_{inj} in L2/3I and L5P: 1.4±1.3%; Z=2.7; I_{inj} in SBC, L2/3I and L5P: 70.8±6.3%; Z=2.0; n=9), and ENGC (I_{inj} in L5P: 62.5±5.3%; I_{inj} in ENGC and L5P: 13.8±5.1%; Z=2.9; I_{inj} in L2/3I and L5P; Z=2.8: 2.5±1.7%; I_{inj} in ENGC, L2/3I and L5P: 0.0±0.0%; Z=2.8; n=10) interneuronal circuits. Note larger uIPSPs induced by the synchronized firing in ENGCs and their targeting L2/3 interneurons (recorded in L5 pyramidal neurons at resting membrane potentials) (ENGC↔L2/3I: 0.55±0.07 mV; ENGC: 0.25±0.04 mV; Z=2.8; L2/3I: 0.33±0.05 mV; Z=2.8; n=10, p<0.01; Wilcoxon tests). Asterisks indicate p<0.05 (Wilcoxon tests).

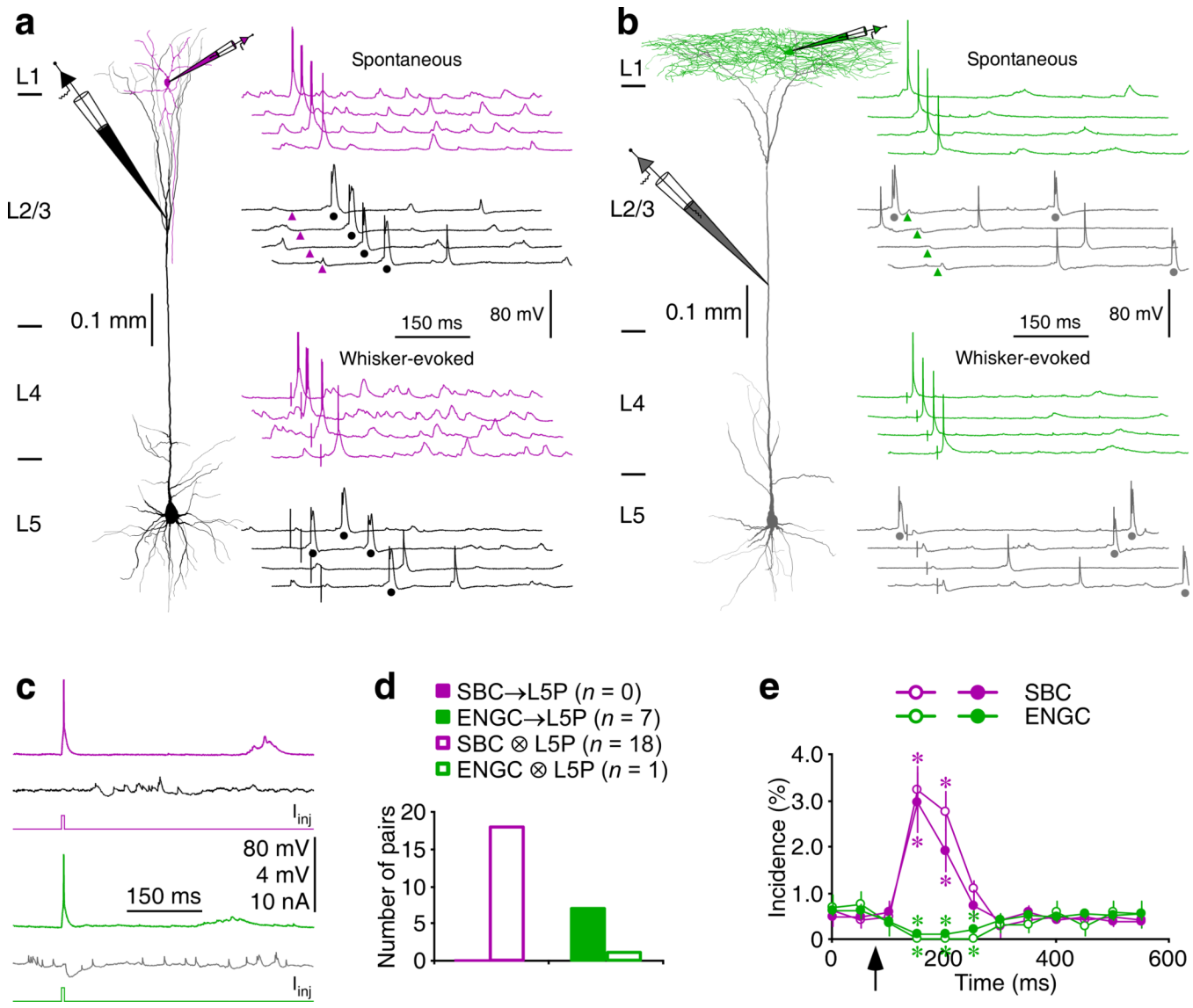

Fig. 8. SBC→ and ENGC↔L2/3I→L5 pyramidal neuronal circuits differ in function *in vivo*

(a–b) Reconstruction of L1 SBC (pink) or L1 ENGC (green) and L5 pyramidal neurons (black or gray) recorded simultaneously in intact animals. Note that the recording traces are aligned by spontaneous somatic action potentials or whisker stimulation, and arrowheads indicate the time of initiation of spontaneous somatic action potentials in simultaneously recorded L1 interneurons and dots indicate the dendritic complex spikes in L5 pyramidal neurons.

(c) The average traces show that the firing in a SBC promoted and that in an ENGC suppressed the initiation of dendritic complex spikes (appeared as spikelet-like events due to averaging) recorded in L5 pyramidal neurons. Scale bars in **a**–**c** apply to all recording traces with 80 mV and 2 mV bars applied to traces with and without action potentials, respectively.

(d) Connectivity of synapses formed by SBCs and ENGCs on L5 pyramidal neurons recorded simultaneously in intact brains (SBC→L5P: 0.0%, n=0 of 18 tested connections; ENGC→L5P: 85.7%, n=7 of 8 tested connections; χ^2=21.6; p<0.005; Chi-squared tests).

(e) Time course of SBC-induced promotion (n=3) and ENGC-induced suppression (n=7) of dendritic complex spiking in L5 pyramidal neurons. Note SBC- and ENGC-mediated effects

(spontaneous and whisker-evoked effects in pink and green and current pulse-evoked effects in dark magenta and dark green) and arrow indicating the time of somatic action potential initiation in L1 interneurons. Note that ENGC-mediated $GABA_B$ responses, although small, were effective in inducing a prolonged suppression of dendritic complex spiking, consistent with employment of a calcium conductance-suppression mechanism[50]. Asterisks indicate $p<0.05$ ($U=0.0$; Mann-Whitney Rank Sum tests).